RSC Advances

PAPER

View Article Online
View Journal | View Issue

Cite this: *RSC Adv.*, 2020, **10**, 30907

Smart magnetic nanopowder based on the manganite perovskite for local hyperthermia†

A. V. Pashchenko,[abc] N. A. Liedienov,[*ab] I. V. Fesych,[d] Quanjun Li,[a] V. G. Pitsyuga,[e] V. A. Turchenko,[bf] V. G. Pogrebnyak,[c] Bingbing Liu[a] and G. G. Levchenko[*ab]

Received 6th August 2020
Accepted 6th August 2020

DOI: 10.1039/d0ra06779b

rsc.li/rsc-advances

For many medical applications related to diagnosis and treatment of cancer disease, hyperthermia plays an increasingly important role as a local heating method, where precise control of temperature and parameters of the working material is strongly required. Obtaining a smart material with "self-controlled" heating in a desirable temperature range is a relevant task. For this purpose, the nanopowder of manganite perovskite with super-stoichiometric manganese has been synthesized, which consists of soft spherical-like ferromagnetic nanoparticles with an average size of 65 nm and with a narrow temperature range of the magnetic phase transition at 42 °C. Based on the analysis of experimental magnetic data, a specific loss power has been calculated for both quasi-stable and relaxation hysteresis regions. It has been shown that the local heating of the cell structures to 42 °C may occur for a short time (~1.5 min.) Upon reaching 42 °C, the heating is stopped due to transition of the nanopowder to the paramagnetic state. The obtained results demonstrate the possibility of using synthesized nanopowder as a smart magnetic nanomaterial for local hyperthermia with automatic heating stabilization in the safe range of hyperthermia without the risk of mechanical damage to cell structures.

1. Introduction

In modern science, medical applications related to (i) magnetic separation,[1] (ii) targeted drug delivery to diseased tissues,[2] (iii) the creation of new MRI contrast agents working at the cellular and molecular level for tumor theranostics,[3,4] (iv) tissue engineering and regenerative medicine,[5,6] (v) magnetic hyperthermia[7,8] are of great interest. In each of these applications, a unique combination of the properties for magnetic nanoparticles (MNPs) is to have a small size and to generate heat under an alternating magnetic field (AMF). The MNP size is in the range of ~1–100 nm, which is comparable with the sizes of intracellular biological structures of ~10–100 nm, viruses ~10–200 nm, proteins ~4–50 nm and genes ~2–100 nm.[9] This allows MNP to penetrate into the tissue and affect the physiological processes of the body at the cellular level. The intensity of heating depends both on the properties of the magnetic nanomaterial (dispersion, Curie temperature, coercivity, magnetization), and on the characteristics of the external influence (temperature, exposure time, AMF amplitude and frequency). While local heating above 44 °C, necrosis of muscle tissue occurs in 10 min.[10] To avoid overheating, it is necessary to strictly control exposure time, AMF amplitude and nanoparticle concentration.[11] The risk of tissue overheating is minimized by the intelligent control system for magnetic hyperthermia. The work of the intelligent system is based on the fact that the Curie temperature of the particles is in the safe hyperthermia range of 42–44 °C. Above the Curie temperature, the particle goes into the paramagnetic (PM) state and its heating ceases. Such a nanopowder exhibits the properties of a smart nanomaterial, since it automatically changes its properties depending on external conditions.

The synthesis of such smart nanopowder allows us to solve another complex problem that is associated with intracellular (local) hyperthermia.[12,13] In magnetic hyperthermia, heating of a particle occurs as a result of losses associated with both frictional heating of a particle during its rotation under AMF (Brownian relaxation) and relaxation of magnetization without rotation of the particle (Néel relaxation).[14] In intracellular hyperthermia, a particle *via* the core–shell structure is modified

[a]*State Key Laboratory of Superhard Materials, International Center of Future Science, Jilin University, 130012 Changchun, China. E-mail: nikita.ledenev.ssp@gmail.com*
[b]*Donetsk Institute for Physics and Engineering named after O.O. Galkin, NAS of Ukraine, 03028 Kyiv, Ukraine. E-mail: g-levch@ukr.net*
[c]*Ivano-Frankivsk National Technical University of Oil and Gas, MESU, 76019 Ivano-Frankivsk, Ukraine*
[d]*Taras Shevchenko National University of Kyiv, 01030 Kyiv, Ukraine*
[e]*Vasyl' Stus Donetsk National University, 21021 Vinnytsia, Ukraine*
[f]*Frank Laboratory of Neutron Physics, Joint Institute for Nuclear Research, 141980 Dubna, Russia*

† Electronic supplementary information (ESI) available: Definition of coherent scattering size in the $La_{0.6}Ag_{0.2}Mn_{1.2}O_3$ nanopowder; definition of the particle size distribution function in the magnetic $La_{0.6}Ag_{0.2}Mn_{1.2}O_3$ nanopowder; The A- and B-structural positions, valence and magnetic states of manganese in non-stoichiometric $La_{0.6}Ag_{0.2}Mn_{1.2}O_3$ nanopowder; calculation of the main magnetic characteristics of the $La_{0.6}Ag_{0.2}Mn_{1.2}O_3$ composition for local hyperthermia. See DOI: 10.1039/d0ra06779b

with biocompatible agents and is rigidly attached to the protein structures of the cell.[15] The rotation of such a particle under AMF can lead to mechanical damage and cell death.[16] In order to avoid mechanical damage to cell structures, heating should be carried out only as a result of Néel relaxation. The temperature dependence of the specific loss power (SLP) during the Néel relaxation has a resonant form and increases sharply near the temperature of the magnetic phase transition.[17] Since, the Curie temperature of smart magnetic nanopowder is in the hyperthermia range of 42–44 °C, such powder with the necessary set of magnetic properties can be used for local hyperthermia without the risk of mechanical damage to cell structures. The search for such smart magnetic nanopowder is a topical task for materials science, physics, nanomedicine and nanotechnology.

2. Heating mechanism and composition choice

In the magnetometric method, which is used to estimate the heating efficiency in hyperthermia,[18] the SLP can be obtained from hysteresis losses during magnetization reversal.[19] The hysteresis heating can be observed both in the quasi-stable hysteresis and in the relaxation hysteresis. The main difference in the heating mechanisms is that dissipative processes appear in the relaxation region, which are associated with the appearance of a phase difference between the AMF and magnetization.[20,21] The SLP in single-domain (SD) particles under the AMF is significantly higher than in multidomain (MD) particles.[22] Thus, it is advisable to use a magnetic powder, which should consist of SD soft MNPs with a large magnetization near FM transition temperature.

For SD monodisperse spherical particles in the quasi-stable region, the magneto-field dependence of the specific hysteresis loss w_{sw} is approximated by the following expression:[23]

$$w_{sw}(H) = \begin{cases} 0 & \text{for } H \le H_C \\ 4M_R H_C\left(1 - (H_C/H)^5\right) & \text{for } H > H_C \end{cases}, \quad (1)$$

where M_R is the residual magnetization, H_C is the coercive field, and H is the magnetic field. The SLP in the external AMF is specified by multiplying the w_{sw} by the frequency f of the AMF:

$$\mathrm{SLP}(H, f) = w_{sw}(H) \times f. \quad (2)$$

Heating MNPs in the relaxation hysteresis is associated with the relaxation processes of magnetization. The relaxation time τ_R for soft magnetic particles, which do not rotate and do not move in the AMF, is equal to the Néel relaxation time $\tau_R = \tau_N = \tau_0 \exp(K_{eff}V/k_BT)$, where $\tau_0 \sim 10^{-9}$ to 10^{-13} s is the characteristic relaxation time.[20,24–26] On the hysteresis curves $M(H)$, the inclusion of the relaxation magnetization processes manifests itself in increasing the area of the hysteresis region A, which has an ellipsoidal shape with an increase in the AMF frequency f.[27] In the magnetic hyperthermia for nanosystems with the parameter $\sigma = K_{eff}V/k_BT$, the specific hysteresis loss w_{sw} in the relaxation region is calculated by the following expressions:[20]

$$A = \frac{\pi H_{max}{}^2 M_S{}^2 V}{3k_B T\rho} \frac{\omega\tau_R}{1+\omega^2\tau_R{}^2}, \text{ for } \sigma \ll 1, \quad (3)$$

$$A = \frac{\pi H_{max}{}^2 M_S{}^2 V}{k_B T\rho} \frac{\omega\tau_R}{1+\omega^2\tau_R{}^2}, \text{ for } \sigma \gg 1, \quad (4)$$

where A is equal to w_{sw}, H_{max} is the AMF amplitude, M_S is the saturation magnetization, V is the volume of the particle, ρ is the density, $\omega = 2\pi f$ is the cyclic AMF frequency.

With an increase in the temperature, the heating efficiency of SLP in a quasi-stable hysteresis region decreases in proportion to the multiplication of M_R and H_C (see eqn (1) and (2)) and equals zero at T_C. However, the SLP increases for the relaxation hysteresis near the temperature of the magnetic phase transition (see eqn (4)). This heating mechanism of particles to a Curie temperature is advisable to use as the main mechanism for heating magnetic nanoparticles in local hyperthermia. The search for a soft magnetic material with a Curie temperature t_C = 42–44 °C, a high saturation magnetization near the Curie temperature, and a narrow temperature FM–PM phase transitions is a topical task for both hyperthermia and material science. Summarizing the above, it is possible to establish requirements for the choice of the composition and characteristics of nanopowder that can be used as a smart magnetic material for local hyperthermia: (i) the nanopowder should be a soft magnetic material, (ii) the magnetic nanoparticles should be predominantly in the SD state, (iii) the Curie temperature should be in the t_C = 42–44 °C range, (iv) the nanopowder should have a narrow temperature range of the magnetic phase transition FM–PM, (v) the magnetic nanoparticles should have a large saturation magnetization M_S near t_C, and (vi) the nanopowder should have a lower H_C coercivity with respect to the AMF ($H_{max} > H_C$).

This list of functional properties may be satisfied by rare-earth manganites $La_{1-x}A_xMnO_3$ with a perovskite structure ABO_3,[28,29] where A is a mono- or divalent large A-cation, such Ca^{2+}, Sr^{2+}, Ba^{2+}, K^+, Na^+, or Ag^+. The Curie temperature of these compounds strongly depends on the ratio $Mn_B{}^{3+}/Mn_B{}^{4+}$, so it is quite easy to control it by changing the concentration and valence state of the A-cation to obtain t_C = 42–44 °C.

Great difficulties in finding the magnetic material for local hyperthermia are connected with the fact that they should have a narrow temperature range of the FM–PM magnetic phase transition. An increase in the temperature range of the magnetic phase transition is associated with both the appearance of local antiferromagnetic interactions caused by the Jahn–Teller electron–phonon interaction with orthorhombic distortions,[30] and the magnetic inhomogeneity of the local environment of manganese as a result of the presence of cation $V^{(c)}$ and anion $V^{(a)}$ vacancies.[31,32] Superstoichiometric manganese is an excess manganese, for which the filling factor of the B-position in the molar formula exceeds one. Using NMR ^{55}Mn method,[31] it was shown that superstoichiometric manganese, which fills cation vacancies and completes the B-sublattice of manganese, increases magnetic homogeneity and reduces the temperature range of magnetic ordering. It should be noted that among the compositions with super-stoichiometric manganese of $La_{1-x}Mn_{1+x}O_{3-\delta}$,[33]

$La_{0.7}Sr_{0.3}Mn_{1.1}O_3$,[34] $La_{0.7}Sr_{0.3-x}Bi_xMn_{1.1}O_3$,[35] $(La_{0.7}Ca_{0.3})_{1-x}Mn_{1+x}O_3$,[36,37] $(Nd_{0.7}Sr_{0.3})_{1-x}Mn_{1+x}O_{3-\delta}$,[31] and $La_{0.9-x}Ag_xMn_{1.1}O_3$,[38] the Ag-containing manganites have a Curie temperature which most close to the necessary functional properties of the magnetic material for hyperthermia, *i.e.* $t_C = 42$–44 °C.[39] Therefore, the non-stoichiometric $La_{0.6}Ag_{0.2}Mn_{1.2}O_3$ composition with an increased content of super-stoichiometric manganese is considered here as the basis for the production of smart magnetic nanopowder for local hyperthermia. In addition, on the toxicity of the investigated nanopowder, it should be added that the manganite perovskite nanoparticles show a better colloidal stability, good biocompatibility with cell lines and do not have toxic effects.[40]

3. Methods

The pyrolytic synthesis of $La_{0.6}Ag_{0.2}Mn_{1.2}O_3$ nanopowder was used. As initial components, aqueous solutions of lanthanum nitrate (0.5 mol L^{-1}), manganese nitrate (0.6 mol L^{-1}), and silver nitrate (0.1 mol L^{-1}) were used. The nitrate solutions were mixed in a stoichiometric ratio and evaporated in a water bath at 80 °C for 6 h. Pyrolysis of the dried mixture was carried out at 600 °C. After grinding in an agate mortar, the powder was calcined in an alundum crucible at 800 °C (10 h). Additional synthesizing annealing was performed at 900 °C (20 h). The powder was cooled under conditions of natural heat exchange between the furnace and the environment.

X-ray diffraction studies were performed on a Shimadzu LabX XRD-6000 X-ray diffractometer in Cu K_α-radiation. Additionally, the phase composition and the type of crystal structure of the studied powder was analyzed by X-ray diffractometer MicroMax-007 HF (Rigaku, Japan) in Mo-K_α radiation, $\lambda = 0.71146$ Å. The refinement of crystal structure was carried out with Rietveld analysis,[41] using the FullProf software.[42] The microstructural characterization of the $La_{0.6}Ag_{0.2}Mn_{1.2}O_3$ nanopowder was performed using JEOL JEM-2200FS transmission electron microscopy (TEM). High-resolution TEM (HRTEM) with accelerating voltage of 200 kV was also used to image $La_{0.6}Ag_{0.2}Mn_{1.2}O_3$ nanoparticles. A sample for the TEM analysis was prepared by placing a drop of diluted suspension of particles in acetone onto a carbon coated copper grid. Particle morphology and particle size were determined by scanning electron microscopy (SEM) on an FEI MAGELLAN 400 Scanning Electron Microscope. Magnetic measurements were carried out on a Quantum Design SQUID MPMS 3 SQUED magnetometer in the temperature range from 2 to 400 K and in magnetic fields up to 70 kOe.

4. Results and discussion

4.1. Structure, phase composition, morphology, and the size of nanoparticles

According to X-ray data (see Fig. 1), the crystal structure of the $La_{0.6}Ag_{0.2}Mn_{1.2}O_3$ nanopowder is well described in the framework of rhombohedral $R\bar{3}c$ space group (No. 167). The sample has a small quantity of impurities: Ag (~2%) and $La(OH)_3$ (~2%). The parameters and volume of perovskite unit cell in the hexagonal setup are equal to $a = 5.4969(2)$ Å, $c = 13.297(1)$ Å and $V = 347.96(4)$ Å, respectively. The X-ray density of $La_{0.6}Ag_{0.2}Mn_{1.2}O_3$ with a molar mass of 218.8 g mol^{-1} and an amount of $Z = 6$ molar formulas per unit cell is $\rho_x = 6.266$ g cm^{-3}. The preservation of structural single-phase up to 96% with a large amount of 20% super-stoichiometric manganese and its absence in minor phases indicates its complete dissolution in the perovskite structure with completed manganese B-sublattice.

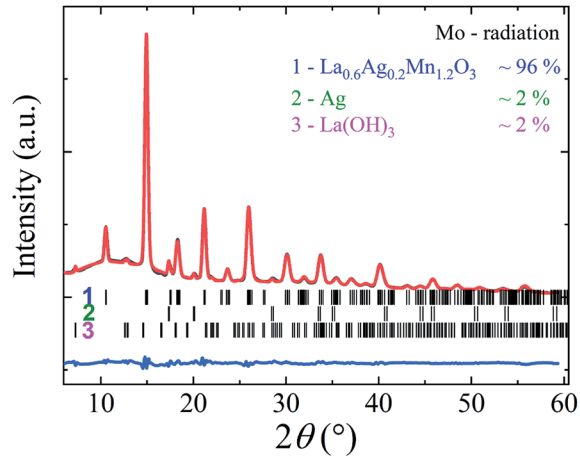

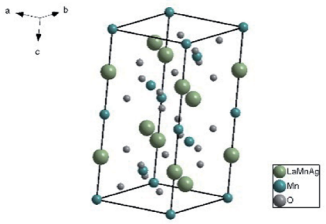

Perovskite $R\bar{3}c$ structure parameters	
a (Å)	5.4969(2)
c (Å)	13.297(1)
V (Å^3)	347.96(4)
La/Ag/Mn (6a)	(0/0/0.25)
Mn (6b)	(0, 0, 0)
O (18e)	(0.4488, 0, 0.25)
R_{exp} (%)	13.35
R_p (%)	11.4
R_{wp} (%)	11.7
χ^2	0.771

Fig. 1 X-ray diffraction pattern of the $La_{0.6}Ag_{0.2}Mn_{1.2}O_3$ sample measured at room temperature and fitted by Rietveld method. The experimental and calculated values (top curves) and a difference curve (the bottom line) normalized to a statistical error are presented. Vertical bars are the calculated positions of diffraction peaks corresponding to the crystal structure of 1 – $La_{0.6}Ag_{0.2}Mn_{1.2}O_3$ (SG $R\bar{3}c$), as well as impurities of 2 – Ag (SG $Fm\bar{3}m$) and 3 – $La(OH)_3$ (SG $P6_3/m$). The general view of perovskite unit cell, as well as atomic coordinates and figures of merit refined with Rietveld method are shown.

According to the SEM and TEM studies, the $La_{0.6}Ag_{0.2}Mn_{1.2}O_3$ nanopowder consists of spherical-like nanoparticles with an average particle size of $D_0^{SEM} = 65 \pm 1$ nm (see ESI 2†) and $D_0^{TEM} \sim 60$ nm (see Fig. 2a), which is in agreement with the XRD, since an average size of the coherent scattering regions is $D_0^{XRD} = 62 \pm 2$ nm (see ESI 1†). HRTEM image of the sample (Fig. 2b) clearly shows the lattice interplanar distance of the $La_{0.6}Ag_{0.2}Mn_{1.2}O_3$ nanoparticles. The Fast Fourier Transform (FFT) using Gatan Microscopy Suite software was used to measure the interplanar distance (see insert in Fig. 2b). Fig. 2c

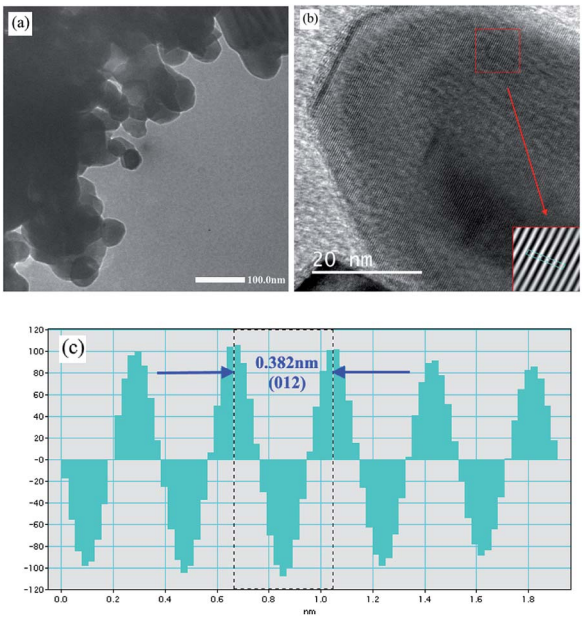

Fig. 2 TEM (a), HRTEM (the insert shows FFT) (b) and lattice plane intensity profile (c) images for determination of shape, size and interplanar distance in the $La_{0.6}Ag_{0.2}Mn_{1.2}O_3$ sample corresponding to (012) plane.

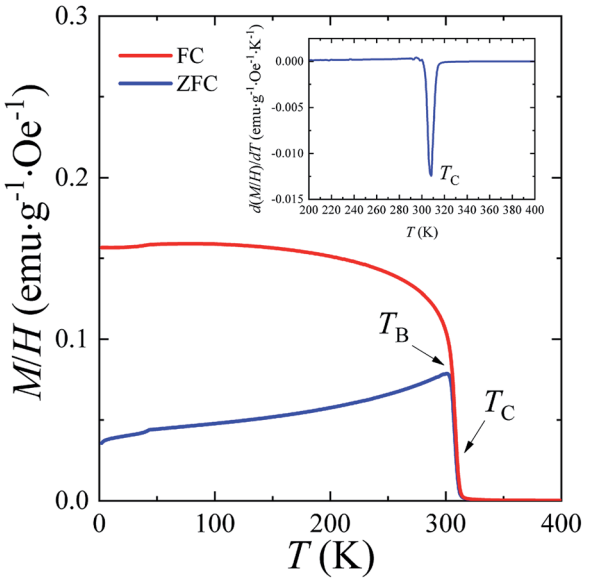

Fig. 3 The temperature dependencies of $(M/H)_{ZFC}(T)$ and $(M/H)_{FC}(T)$ magnetic susceptibility, the Curie temperature T_C and the blocking temperature T_B at $H = 50$ Oe for the $La_{0.6}Ag_{0.2}Mn_{1.2}O_3$ nanopowder.

demonstrates the corresponding lattice plane intensity profile. The interplanar distance of 0.382 nm (012) obtained from FFT is in a good agreement with the XRD data.

The availability of even a slight dispersion in the size D can lead to the magnetic particles being in both the SD and MD states. The magnetic state of a particle affects the magnetic loss of the nanopowder. Establishment of boundary sizes for the $La_{0.6}Ag_{0.2}Mn_{1.2}O_3$ nanopowder, when the transition is observed from one magnetic state to another one, is of interest from a practical point of view for hyperthermia. For this purpose, it is necessary to study the magnetic properties of the $La_{0.6}Ag_{0.2}Mn_{1.2}O_3$ nanopowder in wide temperature and magnetic field ranges.

4.2. Magnetic properties of $La_{0.6}Ag_{0.2}Mn_{1.2}O_3$ nanopowder

The temperature dependences of the $(M/H)_{ZFC}(T)$ and $(M/H)_{FC}(T)$ magnetic susceptibility (see Fig. 3) correspond to a typical manifestation of the magnetic properties of a nanopowder that consists of non-interacting SD FM nanoparticles with randomly oriented uniaxial magnetic anisotropy.[43–45] The Curie temperature $T_C = 308$ K was determined from the temperature dependences of the $d(M/H)/dT$ derivative (see inset on Fig. 3). The blocking temperature $T_B = 301$ K is the maximum of the ZFC curve.[46] For $T < T_B$, the MNPs are in the blocked state. At $T > T_B$, the particles go into superparamagnetic (SPM) unblocked state and the ZFC and FC curves should coincide.[47] Usually, the effective anisotropy constant K_{eff} is determined using a simple its connection with the temperature T_B:[48]

$$K_{eff}V \approx 25k_BT_B. \quad (5)$$

From eqn (5), the constant $K_{eff} = 7.123 \times 10^3$ erg cm^{-3} is calculated for the $La_{0.6}Ag_{0.2}Mn_{1.2}O_3$ nanopowder with the blocking temperature $T_B = 301$ K and the average size of $D_0 = 65.3$ nm for spherical particles.

A more detailed analysis of the ZFC/FC curves made it possible to determine the irreversibility temperature $T_{irr} = 315$ K above of which the temperature hysteresis in the magnetization dependences is completely absent. The $T_B \neq T_{irr}$ condition confirms the result of the SEM studies because there is size dispersion in the $La_{0.6}Ag_{0.2}Mn_{1.2}O_3$ nanopowder. In the ideal case for non-interacting MNPs with the same size D, the blocking temperature T_B and the irreversibility temperature T_{irr} should coincide. In real cases, due to the size dispersion of the particles, the temperature is $T_B < T_{irr}$. It is associated with particles with a large size D, where the blocking temperature T_B is higher according to eqn (5). However, a slight difference between the temperatures of T_B and T_{irr} allows concluding that MNPs with almost the same size take part in the formation of the magnetic properties of the $La_{0.6}Ag_{0.2}Mn_{1.2}O_3$, so the studied nanopowder can be considered to be monodisperse.

Above the temperature T_C, the particles in the $La_{0.6}Ag_{0.2}Mn_{1.2}O_3$ nanopowder go into the PM state, for which the Curie–Weiss law is fulfilled (see Fig. 4):

$$M/H = \frac{C}{T - \theta},$$

where $\theta = 307$ K is the paramagnetic Curie temperature; $C = N\mu_{eff}^2/(3k_B)$ is the Curie constant, $C = 0.015$ emu K (g·Oe)$^{-1}$; N is the number of PM manganese ions, $N = 1$ for a cubic structure; μ_{eff} is the effective magnetic moment of manganese in Bohr magnetons, $\mu_{eff}(Mn) = 4.61\ \mu_B$; μ_B is the Bohr magneton. In a wide temperature range from 316 to 400 K, the linear behavior

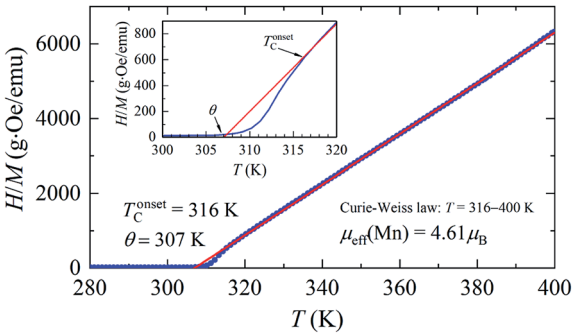

Fig. 4 Temperature dependence of the inverse magnetic susceptibility. The straight red line corresponds to the Curie–Weiss law (θ is the paramagnetic Curie temperature; μ_{eff}(Mn) is the effective magnetic moment of manganese; and T_C^{onset} is the temperature of appearance of FM fluctuations).

of the $(H/M)(T)$ dependency with a high accuracy is approximated by the Curie–Weiss law. Below the temperature of appearance of the FM fluctuations at $T_C^{onset} = 316$ K, the susceptibility deviates from the Curie–Weiss law. This means that in the temperature range from $T_C = 308$ K to $T_C^{onset} = 316$ K (from $t_C = 34$ °C to $t_C^{onset} = 43$ °C), the PM and FM phases coexist. The availability of such regions, where FM fluctuations are observed, may cause heating of the $La_{0.6}Ag_{0.2}Mn_{1.2}O_3$ magnetic powder in AMF to T_C^{onset}.

A very sharp transition to the FM state with a narrow temperature interval ΔT_C (see Fig. 3) due to the influence of super-stoichiometric Mn is of interest because it satisfies the requirements for magnetic powder with an intelligent local hyperthermia control system. The A- and B-structural positions, valence, and magnetic states of manganese in the nanopowder of non-stoichiometric $La_{0.6}Ag_{0.2}Mn_{1.2}O_3$ composition are determined and given in (see ESI 3†).

The magnetic hysteresis loops $M(H)$ in the $La_{0.6}Ag_{0.2}Mn_{1.2}O_3$ nanopowder were measured in a magnetic field up to $H = 70$ kOe at temperatures of $T = 2$, 77, 300, and 400 K (see ESI 3†). The magnetic parameters obtained from hysteresis curves are shown in Table S4 of ESI 3.† With an increase in temperature, the saturation magnetization M_S decreases from $M_S = 69.7$ emu g^{-1} at $T = 2$ K to 65.9 emu g^{-1} at $T = 77$ K and 34.1 emu g^{-1} at $T = 300$ K. At $T = 400$ K, the dependence $M(H)$ is linear, as it should be for the PM state. The coercivity H_C and the residual magnetization M_R also decrease from $H_C = 172$ Oe and $M_R = 7.5$ emu g^{-1} at $T = 2$ K to $H_C = 109$ Oe and $M_R = 4.9$ emu g^{-1} at $T = 77$ K, and to $H_C = 51$ Oe and $M_R = 1.1$ emu g^{-1} at $T = 300$ K.

The magnetization isotherms $M(H)$ of the $La_{0.6}Ag_{0.2}Mn_{1.2}O_3$ nanopowder are presented in Fig. 5. The magnetization process of the MNPs ensemble can be considered as the magnetization of a uniaxial polycrystalline material, for which the law of approximation to the saturation magnetization M_S is valid in a magnetic field H:[49]

$$M = M_S\left(1 - \frac{a}{H} - \frac{b}{H^2} - \frac{c}{H^3} - \ldots\right) + \chi_P H, \quad (6)$$

where a, b, and c are constant coefficients, where only coefficient b is related to the magnetocrystalline anisotropy, and χ_P is

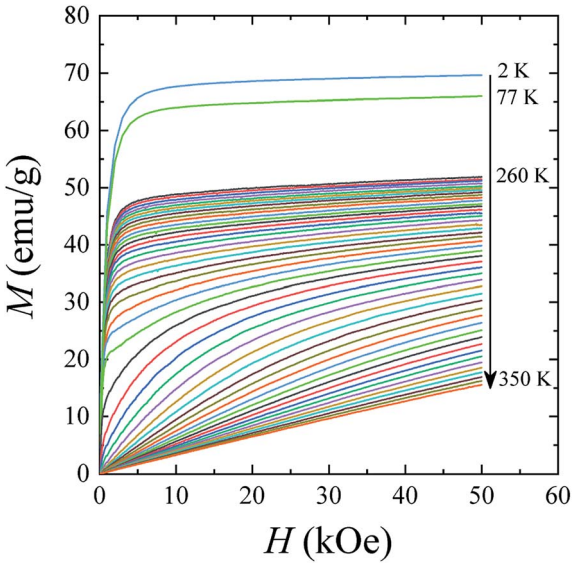

Fig. 5 Magnetization isotherms $M(H)$ for $T = 2$–350 K.

the high field susceptibility. For rare-earth manganites with a cubic crystalline perovskite structure, the coefficient b is:[50]

$$b = \frac{1}{M_S^2}\left(\frac{8}{105}K_1^2 + \frac{4}{15}K_{eff}^{'2}\right),$$

where K_1 is the magnetocrystalline anisotropy constant, $K_{eff}^{'}$ is the effective anisotropy constant that includes the shape anisotropy constant and the magnetostriction constant. For systems with uniaxial anisotropy, the upper limit of K_1 can be obtained from the equality:[51]

$$K_1 = \left[\frac{15}{4}bM_S^2\right]^{1/2}. \quad (7)$$

While approximating the isotherm $M(H)$ for $T = 2$ K by the dependence (6) (see Fig. 6), the coefficient $b = 131.38$ Oe^2 was obtained. Using eqn (7) with a saturation magnetization $M_S = 426.8$ emu cm^{-3} (69.7 emu g^{-1}), the magnetocrystalline anisotropy constant $K_1 = 9.5 \times 10^3$ erg cm^{-3} was obtained.

Using above received parameters of $La_{0.6}Ag_{0.2}Mn_{1.2}O_3$, for making conclusion about possibility to use its for local hypothermia, all necessary for that characteristics were calculated (see ESI 4†) and presented here: magnetic hardness parameter $k = 0.008$, FM exchange length $l_{ex} = 5.476 \times 10^{-7}$ cm, exchange hardness constant $A = 3.432 \times 10^{-7}$ erg cm^{-1}, exchange integral $J_{ex} = 4.63 \times 10^{-15}$ erg and the critical sizes of $D_{cr}^{SD} = 39$ nm for the SD state and of $D_{cr}^{MD} = 51$ nm for the MD state. The values of the parameter k satisfy criterion for the soft magnetic particles. The sizes of D_{cr}^{SD} and D_{cr}^{MD} fully agree with the results of the fundamental work,[52] where the D_{cr}^{MD}/D_{cr}^{SD} ratio for the soft magnetic materials should increase with an increase in the parameter k from 1.2562 at $k = 0$ to ∞ at $k = 0.3253$. Comparing the obtained results with conditions of the magnetic state of nanoparticle, it can be concluded that particles with sizes up to 39 nm are in the SD state (7%), sizes from 39 to 51 nm are in the

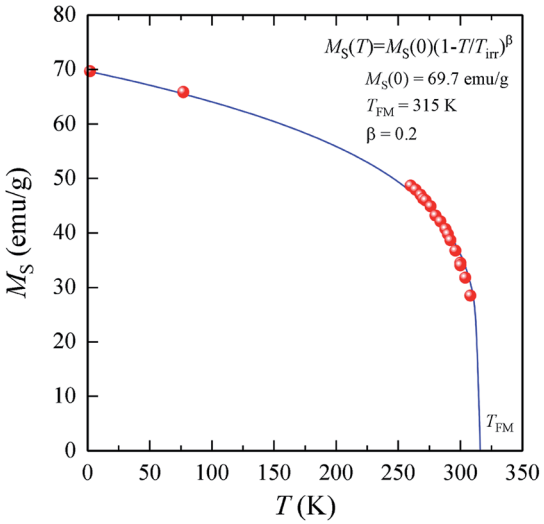

Fig. 6 Spontaneous magnetization of the $La_{0.6}Ag_{0.2}Mn_{1.2}O_3$ nanopowder.

VS state (17%), and sizes of greater than 51 nm are in the MD state (76%) at $T = 2$ K (see ESI 2 and 4†).

According to the Stoner–Wohlfarth model,[53] which considers the properties of non-interacting SD particles with a regular ellipsoidal shape, the anisotropy field H_A can be written as:

$$H_A = 2K_1/M_S. \quad (8)$$

In the Stoner–Wohlfarth model for spherical SD particles at $T = 0$, the anisotropy field coincides with the coercivity, *i.e.* $H_A = H_C$. According to eqn (8), the anisotropy field equals $H_A = 44$ Oe in the $La_{0.6}Ag_{0.2}Mn_{1.2}O_3$ nanopowder with $M_S = 426.8$ emu cm^{-3} and $K_1 = 9.5 \times 10^3$ erg cm^{-3}. For spherical particles with a magnetization of ~400 emu cm^{-3}, even a small deviation from sphericity (the semiaxis ratio in the ellipsoid is 0.9) will lead to an increase in H_C by ~200 Oe.[53] Therefore, the discrepancy between the calculated H_A and experimental H_C is due to the influence of shape anisotropy.

4.3. Heating and temperature stabilization in the $La_{0.6}Ag_{0.2}Mn_{1.2}O_3$ nanopowder

The features of the magnetic behavior of nanoparticles near the magnetic phase transition temperature are of great importance when choosing a smart magnetic nanomaterial for local hyperthermia. Fig. 6 shows the temperature dependence of the saturation magnetization $M_S(T)$, which was plotted based on the analysis of the magnetization isotherms $M(H)$ (see Fig. 5). In the FM region, the $M_S(T)$ curve has the form of a power law:[47]

$$M_S(T) = M_S(0)\left(1 - \frac{T}{T_{FM}}\right)^{\beta}, \quad (9)$$

where $M_S(T)$ and $M_S(0)$ are the spontaneous magnetization at T and at $T = 0$, respectively; T_{FM} is the temperature of FM ordering; and β is the critical coefficient that can take different values for bulk and nanomaterials. $T_{FM} = 315$ K and $\beta = 0.2$ were obtained while approximating the experimental values of $M_S(T)$ by the power dependence (9), where T_{FM} and β were independent parameters taking $M_S(0) = 69.7$ emu g^{-1} into account (see Fig. 6). The approximation was conducted in a wide temperature range from 2 K to $T_C = 308$ K, regardless of the $T_{irr} = 315$ K and $T_C^{onset} = 316$ K temperatures. From the obtained results, the temperature $T_{FM} = 315$ K coincides with the irreversibility temperature $T_{irr} = 315$ K. This coincidence means that the heating magnetic particles can be observed above the transition temperature of MNPs to the SPM state at $T_B = 301$ K up to the $T_{irr} = 315$ K.

In magnetic hyperthermia, a sinusoidal magnetic field can affect the stimulation of peripheral nerves and cardiac tissue.[54] In case of choosing the optimal ranges of the frequency f and the amplitude of the magnetic field H_{max}, it is necessary to take into account their boundary limits, above which the effect of AMF on nervous excitement disappears. The upper stimulation threshold is limited by the range from $H_{max} = 10$ Oe at $f = 100$ kHz to $H_{max} = 10$ kOe at $f = 10$ Hz.[55] This means that for therapeutic purposes it is not recommended to use a sinusoidal magnetic field with low values of f and H_{max}.

On the other hand, in order to avoid the harmful effects of electromagnetic fields on the human body, the upper limit of $f \times H$ should not exceed the maximum value of $(f \times H)_{max}$. In clinical trials, it was found that during hyperthermia for one hour, the subjects did not experience severe discomfort if $(f \times H)_{max} = 6.3 \times 10^7$ Oe s^{-1} (5×10^9 A m^{-1} s^{-1}).[54] AMF with a high frequency causes nonspecific heating in tissues due to the induced eddy currents, which should be minimized. Therefore, it is advisable to consider the possibility of carrying out the hyperthermia procedure in the range of not too high frequencies f with amplitude AMF, which satisfies the condition $f \times H_{max} \leq (f \times H)_{max}$. The results of preclinical studies showed[56] that there were no adverse effects under AFM ($f = 153$ kHz and $H_{max} = 700$ Oe) even with continuous magnetic hyperthermia for 20 minutes. The use of magnetic field with $H_{max} = 1300$ Oe was also acceptable, but keeping heat removal mode with using suitable variations in the duration of electromagnetic pulses.

The heating of SD and monodisperse soft magnetic nanoparticles in the AMF is a result of the hysteresis losses. Fig. 7a shows the temperature changes in the specific loss power, SLP(T), for the $La_{0.6}Ag_{0.2}Mn_{1.2}O_3$ nanopowder under AMF with $H_{max} = 700$ Oe and $f = 90$ kHz. At low temperatures, the SLP values were obtained from experimental hysteresis loops (see Table S4†) for the quasi-stable hysteresis region using eqn (1) and (2). With an increase in the temperature, the SLP decreases from SLP = 46 W g^{-1} at $T = 2$ K to 19 W g^{-1} at $T = 77$ K, 2 W g^{-1} at $T = 300$ K and 0 W g^{-1} at $T = 316$ K. Such a mechanism for heating the magnetic particles does not consider the relaxation processes of magnetization.

The SLP in the relaxation hysteresis region was determined using eqn (2) and (4). In the case, when the relaxation time τ_R depends not only on the volume V of the particle, but also on the magnetic anisotropy K, the temperature dependence $\tau_R(T)$ has the form:[57]

$$\tau_R(T) = \frac{\sqrt{\pi}}{2}\tau_0 \frac{\exp(KV/k_BT)}{\sqrt{KV/k_BT}}. \quad (10)$$

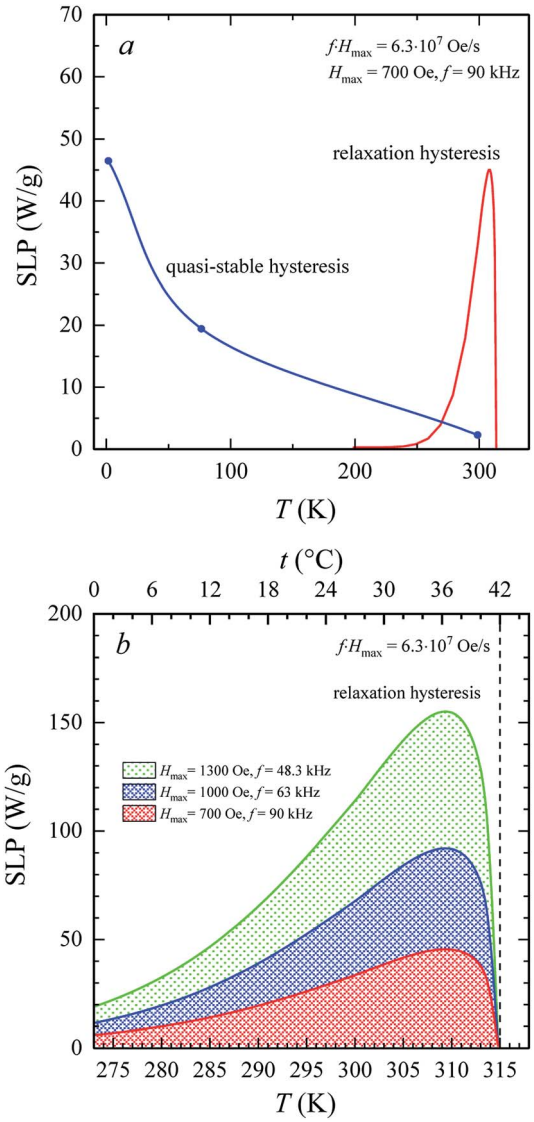

Fig. 7 Temperature changes of SLP in AMF with frequency f and amplitude H_{max} for the $La_{0.6}Ag_{0.2}Mn_{1.2}O_3$ nanopowder: (a) in the quasi-stable (blue curve) and the relaxation (red curve) hysteresis region; (b) near the therapeutic area of hyperthermia. All SLP(T) dependences satisfy the condition $f \times H_{max} = 6.3 \times 10^7$ Oe s^{-1}.

For SPM nanoparticles of lanthanum manganites, the characteristic relaxation time τ_0 is 1.7×10^{-12} s.[58] Calculating SLP near the magnetic phase transition, it is necessary to consider the parameter $\sigma \gg 1$ and the magnetic anisotropy $K = K_{eff}$ for the $La_{0.6}Ag_{0.2}Mn_{1.2}O_3$ nanopowder at $T = 300$ K. The magnetization $M_S(T)$ is a power law dependence (9) with the temperature $T_{FM} = 315$ K and parameter $\beta = 0.2$. As seen from Fig. 7a, at temperatures $T \geq 250$ K, the specific loss power appears and increases. The SLP increases to a maximum value of 44 W g^{-1} at $T = 310$ K and then reduces dramatically to zero at $T = 315$ K. The resulting SLP for the $La_{0.6}Ag_{0.2}Mn_{1.2}O_3$ nanopowder are in good agreement with the specific absorption rate SAR = 48–54 W g^{-1} for manganite $La_{1-x}Sr_xMnO_3$ nanoparticles with $0.2 < x < 0.4$.[57] However, lanthanum–strontium manganite is not suitable to the smart material for magnetic hyperthermia, since it does not have a sharp magnetic phase transition at T_C and the Curie temperature is above the range of 42–44 °C of hyperthermia.[59]

A nonmonotonic behavior of the SLP(T) dependence follows from the relation between the spontaneous magnetization $M_S(T)$ and the relaxation time $\tau_R(T)$ in eqn (4). In the $La_{0.6}Ag_{0.2}Mn_{1.2}O_3$ nanopowder with $\tau_0 = 1.7 \times 10^{-12}$ s, $K_{eff} = 7.123 \times 10^3$ erg cm^{-3} and $D_0 = 65.3$ nm, the relaxation time decreases from $\tau_R = 3.243$ s at $T = 250$ K to 0.024 s at $T = 300$ K and 0.007 s at $T = 315$ K. At a frequency $f = 90$ kHz, taking into account the resonance condition $2\pi f_0 \times \tau_R(T) = 1$, it follows that SLP($T$) should take the maximum value at $T = 490$ K. However, the SLP increases inversely with a decrease in $\tau_R(T)$ within the temperature range from 250 to 310 K, since $M_S(T)$ varies slightly. In the range from 310 to 315 K, a sharp decrease in the SLP is due to a sharp drop in $M_S{}^2$ to 0 (see eqn (4)).

Fig. 7b shows three temperature dependences of SLP(T) in the relaxation hysteresis region for three pairs of values of f and H_{max}. Each SLP(T) curve satisfies the condition for the safe influence of AMF on biological subject, *i.e.* $(f \times H_{max}) = (f \times H)_{max} = 6.3 \times 10^7$ Oe s^{-1}. In all curves, the maximum of SLP is observed at a temperature $T = 310$ K (37 °C). The maximum temperature is independent of H_{max} and f. With an increase in H_{max}, the maximum of SLP increases from 44 W g^{-1} for $H_{max} = 700$ Oe and $f = 90$ kHz to 91 W g^{-1} for $H_{max} = 1000$ Oe and $f = 63$ kHz and up to 153 W g^{-1} for $H_{max} = 1300$ Oe and $f = 48.3$ kHz. Such an increase in SLP by more than 3 times means the possibility of a significant increase in the heating intensity during hyperthermia. This is due to an increase in the amplitude of AMF when heating occurs in the relaxation hysteresis region. It should be also noted that such an increase in SLP occurs without violating the safe influence of AMF on the vital functions of an organism.

For a complete analysis of the functional properties of the smart magnetic $La_{0.6}Ag_{0.2}Mn_{1.2}O_3$ nanopowder, an unclear question remains regarding whether the such power SLP is sufficient to self-heat of MNP and to heat of the cell structures to the therapeutic range at local hyperthermia. Using equation:

$$\Delta t = \frac{\rho_{NP,cell} \times V_{NP,cell} \times c_{NP,cell} \times (t_2 - t_1)}{SLP \times m_{NP}},$$

(Δt is the heating time; $\rho_{NP,cell}$, $V_{NP,cell}$ and $c_{NP,cell}$ are the density, volume and heat capacity of nanoparticle or cell structures, respectively; t_2 and t_1 are the final and initial temperature, m_{NP} is the mass of nanoparticles) and assuming that the entire specific thermal power SLP of a spherical nanoparticle with a mass of 8.9×10^{-16} g (size $D_0 = 65.3$ nm, density $\rho_x = 6.266$ g cm^{-3}) is transferred to cell structures with a size of 500 × 500 × 500 nm (density $\rho_{cell} \approx 1.0$ g cm^{-3} and a specific heat capacity $c_{cell} \approx 4183$ J (kg K)$^{-1}$ for water), then it takes $\Delta t = 79$ s (SLP = 44 W g^{-1}, $H_{max} = 700$ Oe), 39 s (SLP = 91 W g^{-1}, $H_{max} = 1000$ Oe), and 23 s (SLP = 153 W g^{-1}, $H_{max} = 1300$ Oe), to heat one such cell structure at 6 °C from $t_1 = 36$ to $t_2 = 42$ °C. In this case, self-heating of a magnetic nanoparticle will occur in $\Delta t = 0.09$ s for SLP = 44 W g^{-1}, 0.04 s for SLP = 91 W g^{-1}, and 0.03 s for SLP = 153 W g^{-1} ($c_{NP} = 140$ J (mol

K))$^{-1}$.[60] In less than 1.5 min, the magnetic $La_{0.6}Ag_{0.2}Mn_{1.2}O_3$ nanoparticle with minimum SLP = 44 W g^{-1} can increase the temperature of the cell structures, the volume of which is 850 times the volume of the particle itself. It should be also noted that the relaxation mechanism of heating does not cause mechanical damage to cell structures, which can occur during frictional heating as a result of Brownian relaxation. Thus, the synthesized magnetic $La_{0.6}Ag_{0.2}Mn_{1.2}O_3$ nanopowder has desirable functional properties which allow using it as a smart magnetic nanomaterial for the local (intracellular) hyperthermia.

The obtained values of SLP = 44–153 W g^{-1} for the $La_{0.6}Ag_{0.2}Mn_{1.2}O_3$ with a heating rate of 0.1–0.3 °C s^{-1} are comparable to SLP = 26–380 W g^{-1} with a heating rate of 0.3–0.7 °C s^{-1} for Fe_3O_4 and $MnFe_2O_4$ nanoparticles,[61] which are currently used commercially in medical hyperthermia applications. However, the high Curie temperature of T_C = 585 °C for Fe_3O_4,[62] and 277–347 °C for $MnFe_2O_4$,[63] does not allow to automatically stabilize heating in the safe range of hyperthermia (42–44 °C). In addition, the $La_{0.6}Ag_{0.2}Mn_{1.2}O_3$ nanoparticles have an order of magnitude lower coercivity with magnetic hardness parameter k = 0.008 in comparison with Fe_3O_4 and $MnFe_2O_4$, k = 0.01–0.09,[64] that greatly increases the risk of mechanical damage to cells in AMF during intracellular hyperthermia due to using Fe_3O_4 and $MnFe_2O_4$ nanoparticles.

It should be also noted that there are two ^{55}Mn and ^{139}La centers of the NMR signal in the synthesized smart magnetic $La_{0.6}Ag_{0.2}Mn_{1.2}O_3$ nanopowder. In the FM state at $T < T_C$ (42 °C), the formation of the NMR spectrum on ^{55}Mn nuclei (the gyromagnetic ratio γ_{Mn} = 10.560 MHz/T)[65] occurs under the influence of the hyperfine interaction field H_{HIF} = 34–38 T.[36] The field on ^{139}La nuclei (γ_{La} = 6.014 MHz/T)[66] has a dipole–dipole character and is in the range H_{dd} = 2.3–3.7 T.[65,67] In the PM state ($T > T_C$), during MRI studies, the field on the ^{55}Mn and ^{139}La NMR nuclei decreases to ~1.5 T of the tomograph field. Such a variety of magnetic resonance properties of the synthesized $La_{0.6}Ag_{0.2}Mn_{1.2}O_3$ nanopowder operating at the intracellular level additionally opens up great prospects for its use as novel MRI contrast agents for tumor theranostics, which combine the properties of both therapeutic and diagnostic agents.

5. Conclusions

The main ratios of the magnetic and shape-forming parameters of the smart $La_{0.6}Ag_{0.2}Mn_{1.2}O_3$ material suitable for local (intracellular) hyperthermia have been determined. It has been established that the synthesized $La_{0.6}Ag_{0.2}Mn_{1.2}O_3$ nanopowder consists of spherical-like particles with an average size of 65 nm. The main magnetic properties, such as: magnetic hardness parameter, k = 0.008; effective anisotropy constant, K_{eff} = 7.123 × 10^3 erg cm^3; magnetocrystalline anisotropy constant, K_1 = 9.5 × 10^3 erg cm^3; anisotropy field, H_A = 44 Oe (at T = 0); critical size of SD state, D_{cr}^{SD} = 39 nm (at T = 2 K); critical size of MD state, D_{cr}^{MD} = 51 nm (at T = 2 K); Curie temperature, T_C = 308 K; blocking temperature, T_B = 301 K; and temperature of appearance of FM fluctuations, T_C^{onset} = 316 K have been determined for the $La_{0.6}Ag_{0.2}Mn_{1.2}O_3$ nanopowder. These magnetic parameters clearly demonstrate the possibility of using $La_{0.6}Ag_{0.2}Mn_{1.2}O_3$ as a smart magnetic nanomaterial for local (intracellular) hyperthermia. In AMF, the appearance and increase in the SLP near T_C are associated with the influence of the Néel relaxation. Intensive heating of MNPs in the relaxation hysteresis continues up to temperature 42 °C with a maximum value of SLP at t = 37 °C. Such thermomagnetic properties allow locally heating cell structures to 42 °C for a short time, stabilizing this temperature and carrying out magnetic hyperthermia without the risk of overheating and mechanical damage to biological tissue. Obtaining such necessary functional properties has become possible due to the use of the $La_{0.6}Ag_{0.2}Mn_{1.2}O_3$ composition with a super-stoichiometric manganese which demonstrates relaxation hysteresis of magnetization in the temperature range of the magnetic phase transition. Moreover, the presence of ^{55}Mn and ^{139}La NMR centers, as well as unique variety and combination of functional properties in the $La_{0.6}Ag_{0.2}Mn_{1.2}O_3$ nanopowder expand the functionality of using this smart material.

Conflicts of interest

There are no conflicts to declare.

Acknowledgements

This work was partially supported by The Thousand Talents Program for Foreign Experts program of China (project WQ20162200339) and Grant of NAS of Ukraine for research laboratories/groups of young scientists of NAS of Ukraine 2020–2021 (grant agreement no. 08/01-2020).

References

1 K. Y. Castillo-Torres, E. S. McLamore and D. P. Arnold, *Micromachin.*, 2020, **11**, 16, DOI: 10.3390/mi11010016.
2 D. Lombardo, M. A. Kiselev and M. T. Caccamo, *J. Nanomater.*, 2019, **2019**, 26, DOI: 10.1155/2019/3702518.
3 J. Chen, H.-H. Xiang, Z.-Z. Zhao, Y.-K. Wu, M.-Y. Fei and M.-M. Song, *RSC Adv.*, 2020, **10**, 18054–18061, DOI: 10.1039/d0ra01807d.
4 X. Cai, Q. Zhu and Y. Zeng, *Int. J. Nanomed.*, 2019, **14**, 8321, DOI: 10.2147/fijn.s218085.
5 M. Fathi-Achachelouei, H. Knopf-Marques and C. E. Ribeiro da Silva, *Front. Bioeng. Biotech.*, 2019, **7**, 113, DOI: 10.3389/ffbioe.2019.00113.
6 M. Banobre-Lopez, Y. Pineiro-Redondo and M. Sandri, *IEEE Trans. Magn.*, 2014, **50**, 1, DOI: 10.1109/tmag.2014.2.
7 V. M. Kulkarni, D. Bodas and K. M. Paknikar, *RSC Adv.*, 2015, **5**, 60254, DOI: 10.1039/c5ra02731d.
8 D. Chang, M. Lim and J. A. Goos, *Front. Pharmacol.*, 2018, **9**, 831, DOI: 10.3389/fphar.2018.00831.
9 J. Owens Frank and P. Poole Charles, *Physics and Chemistry of Nanosolids*, 2008, vol. 539.
10 M. Dewhirst, B. L. Viglianti and M. Lora-Michiels, *Thermal Treatment of Tissue: Energy Delivery and Assessment II*, 2003, vol. 4954, p. 37, DOI: 10.1117/12.476637.

11 L. Asín, M. R. Ibarra and A. Tres, *Pharm. Res.*, 2012, **29**, 1319, DOI: 10.1007/s11095-012-0710-z.
12 X. Liu, Y. Zhang and Y. Wang, *Theran.*, 2020, **10**, 3793, DOI: 10.7150/thno.40805.
13 C. Blanco-Andujar, D. Ortega and P. Southern, *Nanomedicine*, 2016, **12**, 121, DOI: 10.2217/nnm.15.185.
14 V. M. Kalita, A. I. Tovstolytkin and S. M. Ryabchenko, *Phys. Chem. Chem. Phys.*, 2015, **17**, 18087, DOI: 10.1039/c5cp02822a.
15 N. Zhu, H. Ji and P. Yu, *Nanomaterials*, 2018, **8**, 810, DOI: 10.3390/nano8100810.
16 D.-H. Kim, E. A. Rozhkova, I. V. Ulasov, S. D. Bader, T. Rajh, M. S. Lesniak and V. Novosad, *Nat. Mater.*, 2010, **9**, 165, DOI: 10.1038/nmat2591.
17 G. Barrera, P. Allia and P. Tiberto, *Nanoscale*, 2020, **12**, 6360, DOI: 10.1039/c9nr09503a.
18 Z. Nemati, J. Alonso, L. M. Martinez, H. Khurshid, E. Garaio, J. A. Garcia, M. A. Phan and H. Srikanth, *J. Phys. Chem. C*, 2016, **120**, 8370, DOI: 10.1021/acs.jpcc.6b01426.
19 A. J. Giustini, A. A. Petryk, S. M. Cassim, J. A. Tate, I. Baker and P. J. Hoopes, *Nano LIFE*, 2010, **1**, 17, DOI: 10.1142/s1793984410000067.
20 J. Carrey, B. Mehdaoui and V. Respaud, *J. Appl. Phys.*, 2011, **109**, 083921, DOI: 10.1063/1.3551582.
21 V. M. Kalita, I. Dzhezherya Yu and G. G. Levchenko, *Soft Matter*, 2019, **15**, 5987, DOI: 10.1039/c9sm00735k.
22 A. Jordan, P. Wust, H. Fahlin, W. John, A. Hinz and R. Felix, *Int. J. Hyperthermia*, 1993, **9**, 51, DOI: 10.3109/02656739309061478.
23 R. Hergt, S. Dutz and M. Roder, *J. Phys.: Condens. Matter*, 2008, **20**, 385214, DOI: 10.1088/0953-8984/20/38/385214.
24 E. Lima, E. De Biasi, R. D. Zysler, M. S. Mansilla, M. L. Mojica-Pisciotti, T. E. Torres, M. P. Calatayud, C. Marquina, M. R. Ibarra and G. F. Goya, *J. Nanopart. Res.*, 2014, **16**, 2791, DOI: 10.1007/s11051-014-2791-6.
25 E. A. Perigo, G. Hemery, O. Sandre, D. Ortega, E. Garaio, F. Plazaola and F. J. Teran, *Appl. Phys. Rev.*, 2015, **2**, 041302, DOI: 10.1063/1.4935688.
26 E. Lima, T. E. Torres, L. M. Rossi, H. R. Rechenberg, T. S. Berquo, A. Ibarra, C. Marquina, M. R. Ibarra and G. F. Goya, *J. Nanopart. Res.*, 2013, **15**, 1654, DOI: 10.1007/s11051-013-1654-x.
27 N. A. Usov, M. S. Nesmeyanov and V. P. Tarasov, *Sci. Rep.*, 2018, **8**, 1224, DOI: 10.1038/s41598-017-18162-8.
28 V. Markovich, A. Wisniewski and H. Szymczak, Chapter One Magnetic Properties of Perovskite Manganites and Their Modifications, *Handbook of Magnetic Materials*, Elsevier, 2014, DOI: 10.1016/b978-0-444-63291-3.00001-5.
29 O. A. Shlyakhtin, V. G. Leontiev, O. Young-Jei and A. A. Kuznetsov, *Smart Mater. Struct.*, 2007, **16**, N35, DOI: 10.1088/0964-1726/16/5/n02.
30 J.-M. Li, C. H. A. Huan, Y.-W. Du, F. Duan and Z. X. Shen, *Phys. Rev. B: Condens. Matter Mater. Phys.*, 2000, **63**, 024416, DOI: 10.1103/physrevb.63.024416.
31 A. V. Pashchenko, V. P. Pashchenko, V. K. Prokopenko, F. Revenko Yu, S. Prylipko Yu, N. A. Ledenev, G. G. Levchenko, V. P. Dyakonov and H. Szymczak, *Acta Mater.*, 2014, **70**, 218, DOI: 10.1016/j.actamat.2014.02.014.
32 A. V. Pashchenko, V. P. Pashchenko, V. K. Prokopenko, Y. F. Revenko, A. S. Mazur, V. V. Burchovetskii, V. A. Turchenko, N. A. Liedienov, V. G. Pitsyuga, G. G. Levchenko, V. P. Dyakonov and H. Szymczak, *J. Magn. Magn. Mater.*, 2016, **416**, 457, DOI: 10.1016/j.jmmm.2016.05.010.
33 A. V. Pashchenko, V. P. Pashchenko, Y. F. Revenko, V. K. Prokopenko, A. A. Shemyakov, V. A. Turchenko, V. Y. Sycheva, B. M. Efros, V. P. Komarov and L. G. Gusakova, *Metallofiz. Noveishie Tekhnol.*, 2010, **32**, 487.
34 A. V. Pashchenko, V. P. Pashchenko, Y. F. Revenko, V. K. Prokopenko, A. A. Shemyakov, G. G. Levchenko, N. E. Pismenova, V. V. Kitaev, Y. M. Gufan, A. G. Sil'cheva and V. P. Dyakonov, *J. Magn. Magn. Mater.*, 2014, **369**, 122, DOI: 10.1016/j.jmmm.2014.06.009.
35 A. V. Pashchenko, V. P. Pashchenko, Y. F. Revenko, V. K. Prokopenko, A. S. Mazur, V. A. Turchenko, V. V. Burkhovetskii, A. G. Sil'cheva, P. P. Konstantinov and Y. M. Gufan, *Phys. Solid State*, 2013, **55**, 321, DOI: 10.1134/s1063783413020236.
36 V. P. Pashchenko, A. V. Pashchenko, V. K. Prokopenko, F. Revenko Yu, A. A. Shemyakov and A. G. Sil'cheva, *Tech. Phys.*, 2012, **57**, 1508, DOI: 10.1134/s1063784212110217.
37 A. Sazanovich, J. Pietosa, A. Pashchenko, E. Zubov, V. Dyakonov and H. Szymczak, *Acta Phys. Pol., A*, 2012, **122**, 162, DOI: 10.12693/aphyspola.122.162.
38 A. V. Pashchenko, V. P. Pashchenko, N. A. Liedienov, V. K. Prokopenko, Y. F. Revenko, N. E. Pismenova, V. V. Burhovetskii, V. Y. Sycheva, A. V. Voznyak, G. G. Levchenko, V. P. Dyakonov and H. Szymczak, *J. Alloys Compd.*, 2017, **709**, 779, DOI: 10.1016/j.jallcom.2017.03.093.
39 N. A. Liedienov, V. M. Kalita, A. V. Pashchenko, I. Dzhezherya Yu, I. V. Fesych, Q. Li and G. G. Levchenko, *J. Alloys Compd.*, 2020, **836**, 155440, DOI: 10.1016/j.jallcom.2020.155440.
40 N. D. Thorat, R. M. Patil, V. M. Khot, A. B. Salunkhe, A. I. Prasad, K. C. Barick, R. S. Ningthoujam and S. H. Pawar, *New J. Chem.*, 2013, 372733–372742, DOI: 10.1039/c3nj00007a.
41 H. Rietveld, *J. Appl. Crystallogr.*, 1969, **2**, 65–71, DOI: 10.1107/s0021889869006558.
42 J. Rodrguez-Carvajal, *Phys. B*, 1993, **192**, 55–69, DOI: 10.1016/0921-4526(93)90108-i.
43 F. Tournus and E. Bonet, *J. Magn. Magn. Mater.*, 2011, **323**, 1109, DOI: 10.1016/j.jmmm.2010.11.056.
44 F. Tournus and A. Tamion, *J. Magn. Magn. Mater.*, 2011, **323**, 1118, DOI: 10.1016/j.jmmm.2010.11.057.
45 J.-M. Li, X.-L. Zeng and Z.-A. Xu, *Appl. Phys. Lett.*, 2013, **103**, 232410, DOI: 10.1063/1.4840320.
46 I. J. Bruvera, P. Mendoza Zelis, M. Pilar Calatayud, G. F. Goya and F. H. Sanchez, *J. Appl. Phys.*, 2015, **118**, 184304, DOI: 10.1063/1.4935484.
47 A. V. Bodnaruk, V. M. Kalita, M. M. Kulyk, S. M. Ryabchenko, A. I. Tovstolytkin, S. O. Solopan and A. G. Belous, *J. Phys.:*

Condens. Matter, 2019, **31**, 375801, DOI: 10.1088/1361-648x/ab26fa.

48 C. P. Bean and J. D. Livingston, *J. Appl. Phys.*, 1959, **30**, 120S, DOI: 10.1063/1.2185850.

49 K.-Y. Ho, X.-Y. Xiong, J. Zhi and L. -Z. Cheng, *J. Appl. Phys.*, 1993, **74**, 6788, DOI: 10.1063/1.355078.

50 D. H. Manh, P. T. Phong, P. H. Nam, D. K. Tung, N. X. Phuc and I.-J. Lee, *Phys. B*, 2014, **444**, 94, DOI: 10.1016/j.physb.2014.03.025.

51 D. H. Manh, P. T. Phong and T. D. Tung, *J. Alloys Compd.*, 2011, **509**, 1373, DOI: 10.1016/j.jallcom.2010.10.104.

52 W. F. Brown, *J. Appl. Phys.*, 1968, **39**, 993, DOI: 10.1063/1.1656363.

53 E. C. Stoner and E. P. Wohlfarth, *IEEE Trans. Magn.*, 1991, **27**, 3475, DOI: 10.1109/tmag.1991.1183750.

54 Q. A. Pankhurst, T. K. Thanh and S. K. Jones, *J. Phys. D: Appl. Phys.*, 2009, **42**, 224001, DOI: 10.1088/0022-3727/42/22/224001.

55 J. P. Reilly, *Stimulation via Electric and Magnetic Fields, in Applied Bioelectricity*, Springer, New York, NY, DOI: 10.1007/978-1-4612-1664-3_9.

56 R. Ivkov, S. J. DeNardo and W. Daum, *Clin. Cancer Res.*, 2005, **11**, 7093, DOI: 10.1158/1078-0432.ccr-1004-0016.

57 R. E. Rosensweig, *J. Magn. Magn. Mater.*, 2002, **252**, 370, DOI: 10.1016/s0304-8853(02)00706-0.

58 A. Rostamnejadi, H. Salamati, P. Kameli and H. Ahmadvand, *J. Magn. Magn. Mater.*, 2009, **321**, 3121, DOI: 10.1016/j.jmmm.2009.05.035.

59 Z. Wei, A. V. Pashchenko, N. A. Liedienov, I. V. Zatovsky, D. S. Butenko, Q. Li, I. V. Fesych, V. A. Turchenko, E. E. Zubov, P. Y. Polynchuk, V. G. Pogrebnyak, V. M. Poroshin and G. G. Levchenko, *Phys. Chem. Chem. Phys.*, 2020, **22**, 11817, DOI: 10.1039/d0cp01426e.

60 A. G. Gamzatov, B. Abdulvagidov Sh and A. M. Aliev, *Phys. Solid State*, 2007, **49**, 1769, DOI: 10.1134/s1063783407090260.

61 F. Soetaert, S. K. Kandala, A. Bakuzis and R. Ivkov, *Sci. Rep.*, 2017, **7**, 6661, DOI: 10.1038/s41598-017-07088-w.

62 S. Tikadzumi, *Physics of Ferromagnetism. Magnetic Properties and Practice Applications [in Russian]*, Moscow, Mir, 1987.

63 I. Sharifi, H. Shokrollahi and S. Amiri, *J. Magn. Magn. Mater.*, 2012, **324**, 903–915, DOI: 10.1016/j.jmmm.2011.10.017.

64 Y. O. Tykhonenko-Polishchuk and A. I. Tovstolytkin, *J. Nano-Electron. Phys.*, 2017, **9**, 1–17, DOI: 10.21272/jnep.9(2).02028.

65 A. V. Pashchenko, V. P. Pashchenko, V. K. Prokopenko, A. G. Sil'cheva, Y. F. Revenko, A. A. Shemyakov, N. G. Kisel', V. P. Komarov, V. Y. Sycheva, S. V. Gorban' and V. G. Pogrebnyak, *Phys. Solid State*, 2012, **54**, 767, DOI: 10.1134/s106378341204021x.

66 G. H. Fuller, *J. Phys. Chem. Ref. Data*, 1976, **5**, 835, DOI: 10.1063/1.555544.

67 V. P. Pashchenko, A. V. Pashchenko, A. V. Prokopenko, F. Revenko Yu, V. V. Burkhovetskii, A. A. Shemyakov, A. G. Sil'cheva and G. G. Levchenko, *J. Exp. Theor. Phys.*, 2012, **114**, 503, DOI: 10.1134/s1063776112030193.